

Chimera patterns in conservative systems and ultracold atoms with mediated nonlocal hopping

Hon Wai Lau,^{1,2} Jörn Davidsen,² and Christoph Simon¹

¹*Institute for Quantum Science and Technology and Department of Physics and Astronomy,
University of Calgary, Calgary, Alberta, Canada T2N 1N4*

²*Complexity Science Group, Department of Physics and Astronomy, University of Calgary, Canada T2N 1N4*
(Dated: August 16, 2017)

Chimera patterns, characterized by coexisting regions of phase coherence and incoherence, have so far been studied in non-conservative systems with dissipation. Here, we show that the formation of chimera patterns can also be observed in conservative Hamiltonian systems with nonlocal hopping in which both energy and particle number are conserved. Effective nonlocality can be realized in a physical system with only local coupling if different time scales exist, which can be illustrated by a minimal conservative model with an additional mediating channel. Finally, we show that the patterns should be observable in ultracold atomic systems. Nonlocal spatial hopping over up to tens of lattice sites with independently tunable hopping strength and on-site nonlinearity can be implemented in a two-component Bose-Einstein condensate with a spin-dependent optical lattice, where the untrapped component serves as the matter-wave mediating field. The present work highlights the connections between chimera patterns, nonlinear dynamics, condensed matter, and ultracold atoms.

Introduction

Many interesting dynamical behaviors and physical phenomena observed in nature, including chaos, solitons, and many patterns in spatially extended systems, can only be modeled by nonlinear equations [1–9]. In this context, two fundamental nonlinear differential equations are the complex Ginzburg-Landau equation (CGLE) [1, 2] and the Gross-Pitaevskii equation (GPE) [10–12]. The CGLE corresponds to the normal form of any spatially extended system close to a Hopf bifurcation — a critical point where a stationary system begins to oscillate [2, 3]. It describes many physical systems phenomenologically, such as superconductivity and nonlinear waves [1, 13]. Recently, the study of the CGLE with nonlocal diffusive coupling led to the discovery of an interesting dynamic pattern known as chimera states [5, 14–22]. These states have been experimentally demonstrated in mechanical, chemical, electronic, and opto-electronic systems [23–32]. Chimera patterns are characterized by the coexisting of spatially localized regions of phase coherence and phase incoherence, even in a system with translational symmetry and starts from regular initial conditions. So far, these patterns have been exclusively observed in dissipative or non-conservative systems.

The GPE was derived as a mean-field description of interacting Bose-Einstein condensates (BECs) [33–36]. It is the Schrödinger equation but includes extra nonlinearity. In contrast to the CGLE, it describes a conservative system that locally behaves like an undamped oscillator. Both field equations have global phase symmetry, a third-order nonlinearity, and become equivalent in certain limits [1, 4]. With these similarities, it is natural to ask whether chimera patterns could also be observed for systems described by the GPE. Here, we show that the answer is affirmative. Our work can be considered as a Hamiltonian formulation of chimera states, following a similar attempt for synchronization [37]. Specifically, we show the formation of chimera core patterns consisting of an incoherent core surrounded by a coherent background.

We find that these chimera patterns exist in the two-component GPE under certain conditions, if there is nonlocal hopping (beyond nearest neighbor) with a new characteristic length scale R . Nonlocal descriptions are often conveniently employed for systems such as gravitational, electric, magnetic, and dipole interactions, despite locality being one of the basic principles of physics. These descriptions are accurate when the mediating field is much faster than the dynamics of the particles, so that the mediating picture can be reduced to an effective particle-particle description with a nonlocal term. Similar effective descriptions can be engineered by adding a mediating channel such as the cavity-mediated global coupling [38]. Moreover, the range of coupling may be tunable in certain systems such as those with nonlocal diffusive coupling [39] or long-range coupling mediated by light, [40, 41] studied recently. Tunable hopping [42–45] has also recently been studied as an extension to Bose-Hubbard model (BHM), in contrast to the direct hopping that is usually studied in the BHM [46–48]. The physics of systems that display both nonlocal hopping and nonlinearities are still rarely studied.

In this paper, we introduce three conservative Hamiltonian systems of different levels of generality that show chimera patterns. The first mathematical and most general model is the nonlocal hopping model (NLHM), which can be considered to be the generalization of the discrete GPE with nonlocal hopping, or the mean-field of the BHM with

nonlocal hopping. Then we explain the origin of the effective nonlocal hopping from a minimal model with only local coupling. By attaching a fast mediating channel such that particles can be converted to, the adiabatic elimination of the fast channel results in the continuum NLHM. Finally, the specific physical model we propose is based on a two-component BEC in a spin-dependent trap [49] with Rabi oscillations [50, 51]. In this setup, the hopping originates from the spreading of wavefunctions in the mediating channel governed by a Schrödinger-like equation, so the spatial hopping of atoms is mediated by the matter-wave itself. For this, we employ a mathematical formulation different from previous studies [42, 43]. Our formulation also shows that the main effect of the additional cross-nonlinearity between different components can change the hopping range.

Implementation in BECs has the advantages of exploring both quantum and classical regimes, in addition to allowing flexible control of almost all parameters [52, 53]. For example, adjusting the particle density and the magnetic field near Feshbach resonances [54] can change both the rate of particle loss and the strength of nonlinear interactions. The loss of ultracold atoms limits the lifetime (which can be critical in certain systems [55]) and, in our proposal, limits the maximum observable range of hopping. The difficulty in this implementation is to find the relevant conditions for non-trivial hopping ranges, which is detailed in the later parts of this paper.

Results

Nonlocal hopping model

Hamiltonian and dynamic equation

This most general model is given by the Hamiltonian:

$$\mathcal{H} = \mathcal{U} + \mathcal{P} = \frac{U}{2} \sum_i |a_i|^4 - P \sum_{i,j} G_{ij} a_i^* a_j \quad (1)$$

where $a_i = \sqrt{n_i} e^{i\theta_i}$ is a complex number representing the state of site i , such that $n_i = |a_i|^2$ is the number of particles and θ_i is the phase. \mathcal{U} is the nonlinear energy with the on-site nonlinear interaction U , and \mathcal{P} is the hopping energy with the hopping strength P . G_{ij} is the hopping kernel describing the hopping from site \mathbf{r}_j to \mathbf{r}_i , with $G_{ij} = G_{ji}$. Typically, G_{ij} decreases as the distance $|\mathbf{r}_j - \mathbf{r}_i|$ increases and may be characterized by a hopping range R . For sufficiently small R , the hopping effectively becomes nearest neighbor. This Hamiltonian conserves both the energy and the particle number $N = \sum_i n_i$. It can also be expressed using the canonical coordinate and momentum $\{q_i, p_i\}$, as well as action and angle variable $\{n_i, \theta_i\}$ (see SM sec. S1). Note that the hopping term is quadratic $a_i^* a_j$ in the Hamiltonian, which is different from the usual quartic term of a particle-particle interaction $n_i n_j$ for, say, the Coulomb interaction. Therefore, the corresponding dynamical equation contains the lowest order on-site nonlinearity and the nonlocal linear hopping term:

$$i\hbar \dot{a}_i = U |a_i|^2 a_i - P \sum_j G_{ij} a_j \quad (2)$$

Note that this equation is the mean-field equation of the BHM with nonlocal hopping [42, 43]. Moreover, the nearest-neighbor variation of this equation is the discrete GPE [8] and the non-spatial variation is the discrete self-trapping equation [9].

The dynamic equation of the NLHM can be rewritten in a dimensionless form using the rescaling $a_i \rightarrow a_i / \sqrt{n_0}$, $t \rightarrow (Un_0/\hbar)t$, and $P \rightarrow P/(Un_0)$ where n_0 is the average number of particles per site. The equation becomes: $i\dot{a}_i(t) = |a_i|^2 a_i - P \sum_j G_{ij} a_j$, which depends only on the control parameters of rescaled hopping strength P and rescaled hopping radius R .

Chimera patterns in NLHM

With uniform distribution $a_i = \sqrt{n_0}$, the energy per particle is: $\mathcal{H}/N = Un_0^2/2 - Pn_0$. We consider the initial condition that is an excited state with $|a_i| = 1$ and the spiral phase as shown in Fig. 1a (See Methods). With this initial condition, the system can spontaneously evolve into a state with a small incoherent core surrounded by a large spatially coherent region as shown in Fig. 1b for the phase field. Moreover, the density is randomized near the same

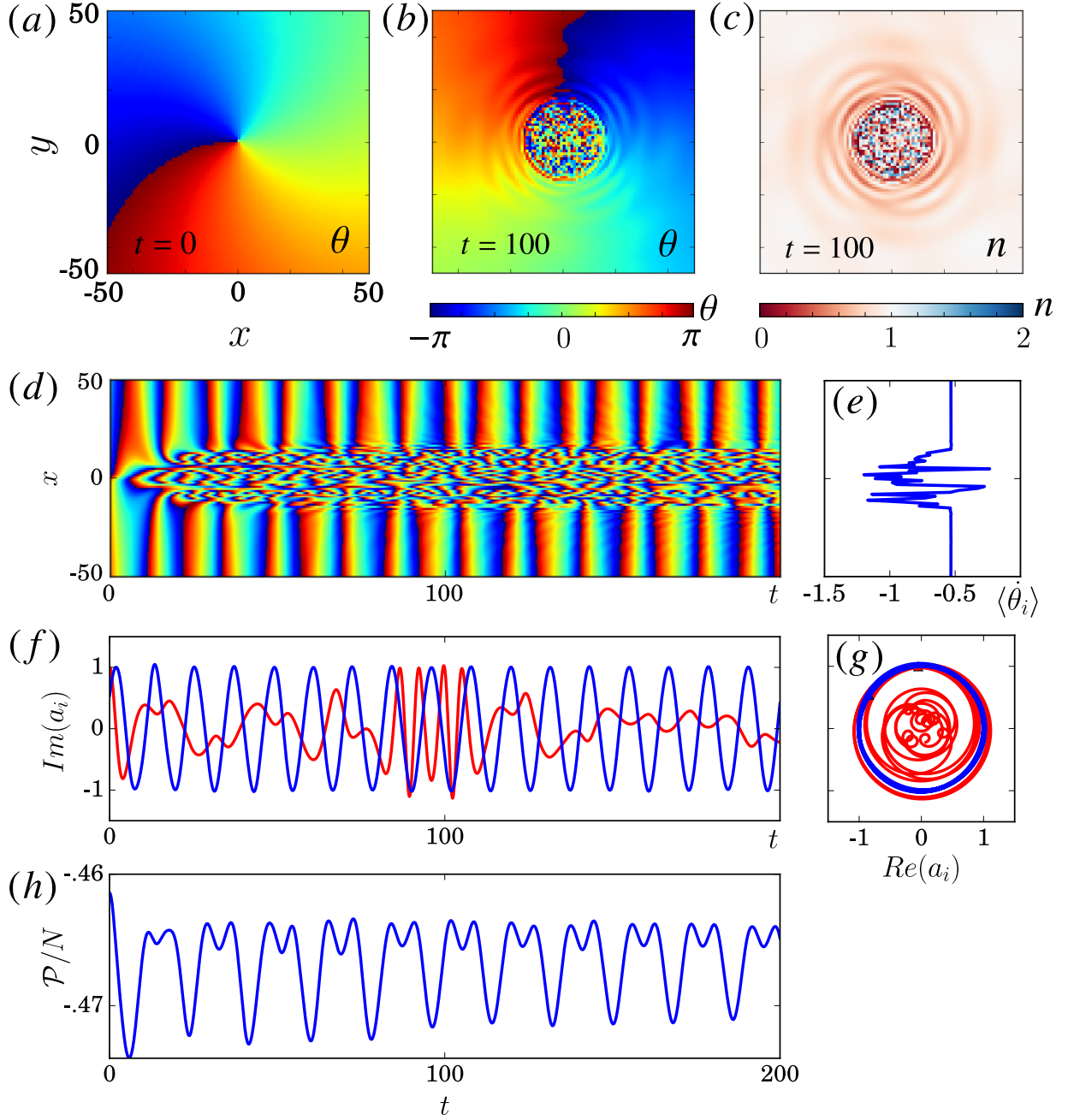


Figure 1: Chimera patterns in the 2D NLHM given by Eq. (1). (a) The initial phase with uniform amplitude $|a_i| = 1$ at time $t = 0$. (b,c) Phase θ_i and number of particle $n_i = |a_i|^2$ at $t = 100$. (d) Time evolution of the phase $\theta_i(t)$ for the cross-section $y = 0$. (e) Averaged local rotation speed $\langle \dot{\theta}_i \rangle$ over the time interval in (d). (f) Time evolution of the points near the center $(x, y) = (-5, 0)$ (red) and far away $(-100, 0)$ (blue). (g) Local phase space trajectory of (f). (h) Hopping energy per particle \mathcal{P}/N variation over time. Parameters: $Un_0 = 1$, $P = 0.5$, $R = 16$, and size $L = 256$ with no-flux boundary condition. Only the core region is shown for clarity. The hopping kernel G_{ij} is given in Table I. Dimensionless units and $\hbar = 1$ are used.

core region in Fig. 1c. As shown by the dynamics of a cross-section in Fig. 1d, this spatial structure is sustained over long times (see also SM and animation). The local dynamics of the two oscillators in Figs. 1f and 1g clearly show the difference between two regions: a_i oscillates regularly far from the core, but not close to it. The incoherent core size scales linearly with the hopping range R and only appears if it is sufficiently large $R \gtrsim 3$. Moreover, with nearest-neighbor hopping, the system reduces to the discrete GPE so that the incoherent region spreads out and interferes like a wave (see SM Fig. S3 and S4). All of these features are consistent with previous observations of chimera cores for driven-dissipative systems with self-sustained oscillators [17, 18, 21]. Other features are, however, distinct. Specifically, the time-averaged angular speed $\langle \dot{\theta}_i \rangle$ behaves non-monotonically across the incoherent core (see Fig. 1f), whereas it typically changes monotonically with distance from the incoherent core in the dissipative case [18, 20]. More importantly, as a conservative Hamiltonian system, it has time reversal symmetry and it conserves of both quantities \mathcal{H} and N . This leads to persistent fluctuations or ripples as observed in Figs. 1b-d, which would be damped away in a dissipative system quickly. In addition, the results of the backward time evolution of the core region is very delicate. With a small perturbation, the background can evolve back to nearly the same state at $t = 0$, but the core remains incoherent, which again signifies the difference between two regions (see SM and animation). This suggests that the Poincare recurrence time to a regular spiral is large and that the probability to encounter a regular spiral is zero in the infinite system size limit. Moreover, the nonlinear energy \mathcal{U} and hopping energy \mathcal{P} are well-defined and both change over time as shown in Fig. 1h for this excited state. Note that the total energy \mathcal{H} is constant with $\mathcal{H}/N \approx 0.0386$. In realistic experimental systems, a small amount of particle loss typical exists and can be modeled phenomenologically by an additional term $U \rightarrow U - iU_{\text{loss}}$. Intuitively, the dynamics should not change significantly if the loss of the particles is less than half of the initial number of particles given by the condition $U_{\text{loss}}t/\hbar \lesssim 1$, but the time also needs to be long enough for the chimera pattern to form. For example, chimera patterns can still be observed with $U_{\text{loss}}/U = 0.02$, see SM sec. S4 for details.

Mechanism for nonlocal hopping and the minimal model

Mediating mechanism

The key idea for the mediating mechanism is to attach an inter-convertible mediating channel (labelled by ψ_2) to trapped states (labelled by ψ_1) as illustrated in Fig. 2a. With direct hopping, increasing the energy barrier between neighboring sites decreases both the hopping strength and the hopping range together. In contrast, if the particles can be converted into fast mediating states that do not experience any energy barrier, then the particles can physically jump much further away. Mathematically, this channel can be eliminated adiabatically, resulting in an effective nonlocal model (see Fig. 2b) with independently adjustable on-site nonlinearity, hopping strength, and hopping range that can be tuned from nearest-neighbor to global hopping.

Minimal model

A minimal mathematical model that captures the concepts of the mediating channel discussed above takes the form:

$$i\hbar\dot{\psi}_1(\mathbf{r}, t) = U|\psi_1|^2\psi_1 + \hbar\Omega\psi_2 \quad (3a)$$

$$i\hbar\dot{\psi}_2(\mathbf{r}, t) = -\hbar\kappa\nabla^2\psi_2 + \hbar\Omega\psi_1 + \hbar\Delta\psi_2 \quad (3b)$$

for the localized ψ_1 and mediating ψ_2 components respectively. The corresponding Hamiltonian is given in the next subsection. The inter-conversion is governed by a coherent coupling with Rabi frequency Ω and a detuning Δ that conserves the number of particles [50, 51]. Eq. (3b) is essentially the Schrödinger equation for free particles with inverse mass $\kappa = \hbar/(2m) > 0$ and so the particles can propagate outward. The additional detuning in the far-detuned regime $|\Delta| \gg |\Omega|$ can ensure the mediating idea is well-defined: The number of particles $N_j = \int d\mathbf{r}|\psi_j|^2$ in the mediating channel $N_2 \ll N_1 \approx N$ can be neglected. Note that this model is not captured by the framework of nonlocal diffusive coupling [39].

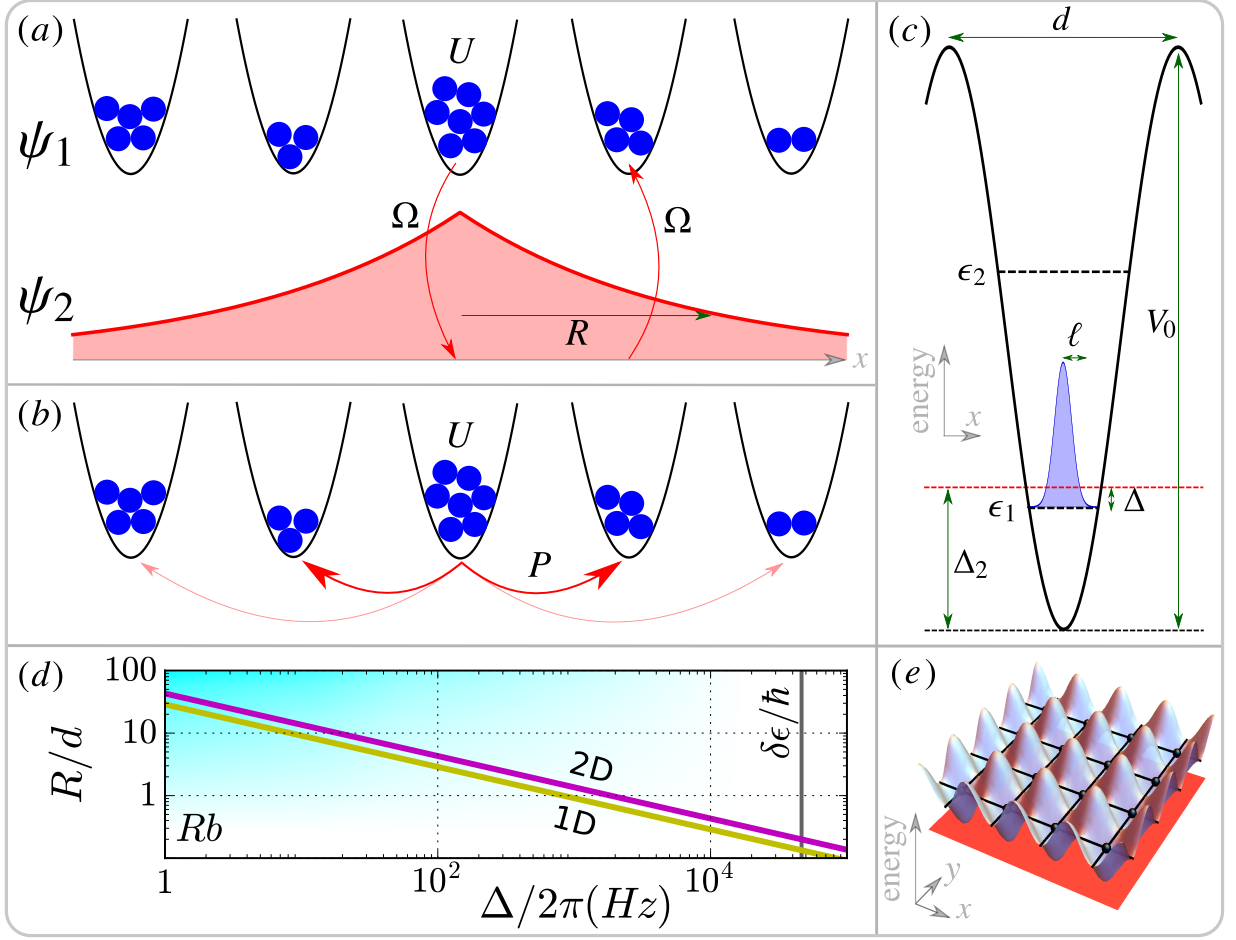


Figure 2: Illustration of mediated hopping. (a) Two-component model: Particles with on-site interaction U are trapped (denoted by ψ_1) but can be converted into a mediating state (denoted by ψ_2) that can propagate freely. It is eventually converted back to nearby sites, giving rise to a characteristic hopping range R . (b) Effective model with hopping strength P after adiabatically eliminating the fast mediating channel. (c) Periodic lattice with spacing d and lattice depth V_0 : Trapped bosonic particles can be described by local ground state wavefunctions with width ℓ and energy ϵ_1 (with energy gap $\delta\epsilon = \epsilon_2 - \epsilon_1$). P and R can be controlled by the Rabi frequency Ω and the detuning $\Delta = \Delta_2 - \epsilon_1/\hbar$ between localized states and mediating states. (d) R can be adjusted by Δ , see text for details. (e) 2D periodic lattice considered in Fig. 4.

Table I: The D -dimensional Green's function $G_D(r)$ with $r = |\mathbf{r}_j - \mathbf{r}_i|$. K_0 is the modified Bessel function of the second kind.

	$D = 1$	$D = 2$	$D = 3$
G_D	$e^{-r/R}$	$K_0(r/R)$	$\frac{1}{r}e^{-r/R}$

Adiabatic elimination

Suppose ψ_1 evolves much slower than ψ_2 , then we can apply adiabatic elimination by setting $\dot{\psi}_2 = 0$ [57]. The solution of $-\kappa\nabla^2\psi_2 + \Omega\psi_1 + \Delta\psi_2 = 0$ in the unbounded isotropic space with translation invariant is given by the convolution $\psi_2(\mathbf{r}, t) = -(\Omega/\Delta)G_D(\mathbf{r}) * \psi_1(\mathbf{r}, t)$, where $G_D(\mathbf{r})$ is the D -dimensional hopping kernel as listed in Table I, with hopping radius $R = \sqrt{\kappa/|\Delta|}$. Note that $\Delta > 0$ is required for the solution of confined hopping kernels (see the form of ψ_2 in Fig. 2a), while $\Delta < 0$ leads to wave-like solution. Substituting this solution back into Eq. (3a), we

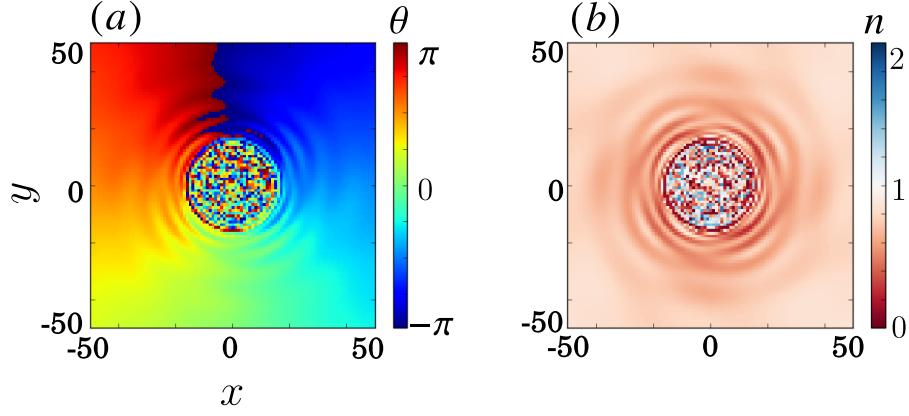


Figure 3: Chimera patterns in the minimal model given by Eq. (1) at $t = 100$ similar to Fig. 1b-c. The setting is the same as in Fig. 1 but with parameters $\Delta = 16$, $\Omega = \sqrt{8}$, $U = 1$, and $\kappa = 4096$.

can get the continuum NLHM:

$$i\hbar\dot{\psi}(\mathbf{r}, t) = U|\psi|^2\psi - P \int d\mathbf{r}' G(\mathbf{r}, \mathbf{r}')\psi(\mathbf{r}', t), \quad (4)$$

where the summation is replaced by an integral with hopping strength $P = \hbar\Omega^2/\Delta$. As shown in Fig. 3, the continuous NLHM well-approximates the discrete NLHM results from Fig. 1.

Mediated hopping in ultracold atomic systems

Hamiltonian and dynamic equation

An ultracold atomic system of a general two-component GPE in a spin-dependent trap with coherent conversion is given by the Hamiltonian:

$$\mathcal{H} = \sum_{i=1,2} \left(\mathcal{H}_i + \frac{1}{2}\mathcal{U}_{ii} \right) + \mathcal{U}_{12} + \mathcal{R}, \quad (5)$$

with

$$\mathcal{H}_i = \int d\mathbf{r} \left(\frac{\hbar^2}{2m_i} |\nabla\psi_i(\mathbf{r})|^2 + V_i(\mathbf{r})|\psi_i(\mathbf{r})|^2 \right), \quad (6)$$

$$\mathcal{U}_{ij} = g_{ij} \int d\mathbf{r} |\psi_i(\mathbf{r})|^2 |\psi_j(\mathbf{r})|^2, \quad (7)$$

$$\mathcal{R} = \sum_{i=1,2} \hbar\Delta_i \int d\mathbf{r} |\psi_i(\mathbf{r})|^2 + \hbar\Omega \int d\mathbf{r} (\psi_1^*(\mathbf{r})\psi_2(\mathbf{r}) + \psi_2^*(\mathbf{r})\psi_1(\mathbf{r})), \quad (8)$$

and with the normalization $N = N_1 + N_2$ where $N_i = \int d\mathbf{r} |\psi_i(\mathbf{r})|^2$ is the number of particles for each component. m_i is the mass of the particles, $V_i(\mathbf{r})$ is the trap potential, g_{ij} is the two-particle collision coefficient, and we assume $g_{12} = g_{22} = 0$ for the moment (see explanation below for non-zero case). The Rabi oscillation term \mathcal{R} represents the inter-conversion between the two components with the spatially homogeneous Rabi frequency Ω and the detuning Δ_i . By setting $V_i = 0$, $m_1 \rightarrow \infty$, and $\Delta_1 = 0$, we arrive at the Hamiltonian for the minimal model discussed above. When a small nonlinearity exists in the mediating channel, the effective detuning becomes $\Delta \rightarrow \Delta + g_{12}|\psi_1|^2 + g_{22}|\psi_2|^2$ if ψ_i is uniform. Hence, the hopping radius decreases for $g_{ij} > 0$ which is typical for atomic systems.

Mathematically, Eq. (3a) can be obtained by setting appropriate parameters for the system described by Eq. (5). In particular, the absence of kinetic energy term in Eq. (3a) requires $m_1 \rightarrow \infty$. However, the mass m of inter-convertible atomic systems are the same, so $m_i = m$. To circumvent this, we can increase the effective mass; for example, by

placing the atoms in a periodic lattice. This can be achieved by additionally setting $V_2 = 0$, V_1 to be periodic, and $\Delta_1 = 0$. Then the dynamic equation becomes [58]:

$$i\hbar\dot{\psi}_1(\mathbf{r}, t) = (-\hbar\kappa\nabla^2 + V_1 + g_{11}|\psi_1|^2)\psi_1 + \hbar\Omega\psi_2 \quad (9a)$$

$$i\hbar\dot{\psi}_2(\mathbf{r}, t) = (-\hbar\kappa\nabla^2 + \hbar\Delta_2)\psi_2 + \hbar\Omega\psi_1 \quad (9b)$$

Only the positive detuning $\Delta = \Delta_2 - \epsilon_1/\hbar > 0$ is considered here as illustrated in Fig. 2c.

Mapping to effective NLHM

Note that direct adiabatic elimination does not work if states with high energy $\epsilon_{i>1}$ are occupied. This is because high energy states do not evolve slowly compared to the mediating component. To avoid occupying higher energy levels, we can confine the system to local ground states $\phi(\mathbf{r})$ with energy ϵ_1 and prevent excitation by choosing a suitable detuning such that $\epsilon_2 - \epsilon_1 \gg \hbar\Delta \gg \hbar|\Omega|$ (see Fig. 2c). Under these constraints, along with adiabatic elimination, we can show (sec. S2 in SM) that Eqs. (9a) and (9b) reduce to the exact form of Eq. (2) with $U = g_{11} \int |\phi|^4$, $P = \hbar\Omega^2/\Delta$, hopping kernel $G_D(r)$ in Table I, and

$$R = C_D \left(\frac{d}{2\ell} \right)^{\frac{D}{2}} \sqrt{\frac{\kappa}{\Delta}} \quad (10)$$

for $d \gg 2\ell$, where C_D is a constant. Intuitively, particles staying in the mediating channel for a longer time have a larger hopping range $R \sim \Delta^{-1/2}$. Since the effective conversion region has a characteristic length scale 2ℓ in a unit lattice with length d , scaling with $2\ell/d$ is expected. Indeed, we have the effective scaling $\Delta \rightarrow \Delta_{eff} = (2\ell/d)^D \Delta$. The self-consistency condition for adiabatic elimination is $\hbar\Delta \gg Un_0, P$ assuming all $n_i \sim n_0$ (n_0 is the average number of particles per site). In this effective NLHM, a_i in Eq. (1) represents the state of a localized wavepacket at site i . Moreover, the kernel G_{ij} in Eq. (1) describes the matter-wave mediated hopping with wavepackets annihilated at site j and created at site i .

Optical lattice

Suppose the trapping potential is sinusoidal $V_1(\mathbf{r}) = V_0 \sum_{\sigma} \sin^2(kx_{\sigma})$ with wavelength λ , wavenumber $k = 2\pi/\lambda$, lattice spacing $d = \lambda/2$, and trap depth V_0 . The summation is taken over the lattice trap dimension as shown in Fig. 2c or 2e. For sufficiently large V_0 , all direct hopping can be suppressed, and the local ground states at trap minima can be approximated by a Gaussian $\phi_{\sigma}(x_{\sigma}) = e^{-\pi x^2/(2\ell_{\sigma}^2)}/\sqrt{\ell_{\sigma}}$ with $\ell_{\sigma} = \sqrt{\pi\hbar/(m\omega_{\sigma})}$. In this setting, the nonlinearity is enhanced by the high density since $U = g_{11}/W$ with effective volume $W = 2^{3/2}\ell_x\ell_y\ell_z$. The constant can be found by numerical fitting, which gives $C_D \approx 1$ (sec. S3 in SM).

Achievable hopping range

For the hopping to be considered nonlocal, $R > d$ must be satisfied. An example of Rubidium atoms is shown in Fig. 2d with $d = 395\text{nm}$ and a deep trap $s = 40$ (expressing $V_0 = sE_R$ in recoil energy $E_R = \hbar\kappa k^2$). Typically, with such a large s , the direct hopping can be ignored and the system becomes a Mott insulator in the quantum regime [46]. Nevertheless, mediated hopping can completely replace the direct hopping (with order $R \sim d$, see Fig. 2d) and allow real time control. Since Ω , Δ , and U can be easily adjusted in experiments, there seems to be no upper bound on R . From a practical point of view, however, it is limited by the lifetime τ and experimental duration. A simple estimation of $\tau \sim 1\text{s}$ gives a maximum $R \sim 30d$ as shown in Fig. 2d.

Tuning nonlinearity and loss

The regime with competitive $P \sim Un_0$ is the most interesting. However, a BEC in a 3D optical lattice using the parameters given above has a strong nonlinearity $U/\hbar = 2\pi \times 2.23\text{kHz}$, which demands a large Δ and, consequently, a small R . U can be reduced by the use of two tuning techniques: Decreasing the density, or utilizing the Feshbach

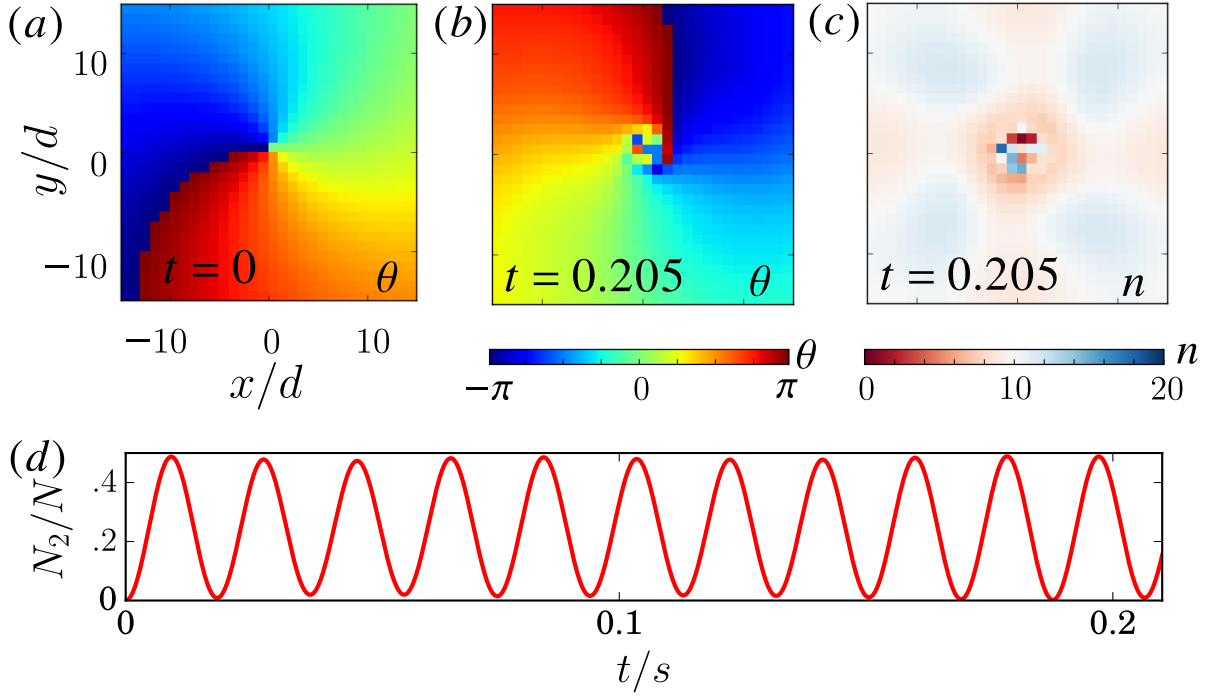


Figure 4: Chimera patterns in BECs. (a) Initial phase θ_i with a uniform number of particles per lattice site $n_i = 10$. (b,c) θ_i and n_i of the state at time $t = 205$ ms. The simulation is based on Eq. (9) in the 2D lattice given by Fig. 2e with $100d \times 100d$ and the no-flux boundary condition. We spatially average over the lattice units. (d) Inter-conversion between two components. For the optical lattice, we use Rubidium ^{87}Rb with $s = 40$ and $d = 395\text{nm}$ which gives $\ell_x = \ell_y = 0.22d$. Additional parameters: $\Delta = 2\pi \times 48\text{Hz}$, $\Omega = 2\pi \times 32\text{Hz}$. The density is decreased by using $\ell_z = 200\ell_x$, and the nonlinearity is weakened 10 times by using Feshbach resonance. The estimated values are $Un_0/\hbar \approx 2\pi \times 19\text{Hz}$, $P \approx 2\pi \times 16\text{Hz}$, $R \approx 6d$, and $\tau \approx 5\text{s}$.

resonance. The latter method can experimentally tune the nonlinearity over many orders of magnitude [54]. The former method is preferable because both nonlinearity and collision loss can be decreased simultaneously. In 1D and 2D lattices, the non-lattice dimension can be weakly trapped to reduce the density, resulting in a lattice of cigarette-shaped wavefunctions [59, 60]. In this case, the dominant loss is the two-particle loss in the localized component. The rate of the two-particle loss can be estimated by $U_{\text{loss}} = \hbar L_{11}/W$ and therefore half-life $\tau = W/L_{11}$ with two-particle loss rate L_{11} [55]. This implies that $\tau \sim \ell_z$ in 2D, so increasing ℓ_z can improve the BEC lifetime.

Chimera patterns in BECs

The derivation of effective models implies that chimera patterns can also be observed in certain parameter regimes for Eqs. (3) and (9). The question is: can such parameter regimes be achieved experimentally? The possible existence of chimera patterns in ultracold atoms is established in a parameter regime given in Fig. 4, based on a full simulation of Eqs. (9). Similar to Fig. 1, a random core appears eventually. Fig. 4d shows the Rabi oscillation between the two components with frequency $\sim \sqrt{\Omega^2 + \Delta^2}$. Note that most of the atoms can be converted back after a full period, which confirms the physical picture discussed in Fig. 2a and is consistent with previous works [42, 43]. We also observe chimera patterns in both the far-detuned regime and the regime with $\Delta \sim \Omega$, which may not be well-described by an effective NLHM.

Experimentally, the initial state can be prepared from a uniform BEC, with V_1 adiabatically turned on until the direct hopping is suppressed and mediated hopping begins to dominate. The energy shift induced by a short light-pulse can then be used to create any desired initial phase. The system states and dynamics may be detected by using various techniques such as optical readout, time of flight techniques, or matter-wave interference [61, 62]. The loss $U_{\text{loss}}/U \approx 0.017$ here is comparable with the discussion in the minimal model. Note that a small amount of loss can cause the BEC system to follow the classical trajectory [63], and so each site can be well-described by a classical

mean-field amplitude and phase. All of this suggests that chimera patterns should be observable in experimental BECs.

Discussion

In summary, we have shown the formation of chimera patterns in three conservative Hamiltonian systems. The NLHM is a direct analogue of the nonlocal CGLE [14], in that both systems have a third-order nonlinearity, nonlinearity, except that the nonlocal diffusive coupling in the CGLE is replaced by nonlocal hopping in the NLHM. The nonlocal hopping requires the underlying physical model to conserve both the energy and particle number, as is typical in ultracold systems. The results of our simulations that used realistic parameters suggest that chimera patterns should be observable in the experiments of ultracold systems.

Our results in this paper are based on the classical conservative Hamiltonian, which provides a new avenue to understand chimera patterns. These results may be extended into the quantum regime, since all of the physical processes that we analyzed are coherent and conserve both energy and particles. Eq. (1) - (9) can be quantized, and Eq. (1) becomes the Bose-Hubbard model with tunable mediated hopping [42]. This opens the door for the exploration of exotic condensed-matter states, such as supersolid states, in addition to other long-range effects [48, 64]. The technique that we presented suggests that experimental studies of the synchronization and chimera patterns of a large number of oscillators may be feasible in quantum systems [65–70]. We hope that our work here motivates further studies on chimera states and mediated nonlocal hopping.

Methods

The numerical methods we used are the fourth-order time splitting method for Gross-Pitaevskii equations [71]. This method for the conservative systems automatically conserve the particle number. For systems with particle loss, we used the standard fourth-order Runge-Kutta is used. The geometry used in the simulations is a square lattice with size L and the no-flux boundary condition. For the spiral initial condition, uniform density $|a_i| = \sqrt{n_0}$ is used and the state is given by $a_i(t = 0) = \sqrt{n_0}e^{i(k_s r - \tan^{-1}(y/x))}$ with $r = \sqrt{(x^2 + y^2)}$. For the system with a mediating channel, the channel is initially empty $\psi_2 = 0$.

-
- [1] Igor S. Aranson and Lorenz Kramer, “The world of the complex Ginzburg-Landau equation,” *Rev. Mod. Phys.* **74**, 99–143 (2002).
 - [2] Yoshiki Kuramoto, “Chemical Oscillations, Waves, and Turbulence,” (Springer Berlin Heidelberg, 1984) pp. 1–4.
 - [3] Raymond Kapral and K. Showalter, *Chemical Waves and Patterns* (Springer Science & Business Media, 2012).
 - [4] Michael Cross and Henry Greenside, *Pattern Formation and Dynamics in Nonequilibrium Systems*, 1st ed. (Cambridge University Press, 2009).
 - [5] Mark J. Panaggio and Daniel M. Abrams, “Chimera states: coexistence of coherence and incoherence in networks of coupled oscillators,” *Nonlinearity* **28**, R67 (2015).
 - [6] Arkady Pikovsky, Michael Rosenblum, and Jürgen Kurths, *Synchronization: A Universal Concept in Nonlinear Sciences*, 1st ed. (Cambridge University Press, Cambridge, 2003).
 - [7] Steven H. Strogatz, *Nonlinear Dynamics And Chaos: With Applications To Physics, Biology, Chemistry, And Engineering*, 1st ed. (Westview Press, Cambridge, MA, 2001).
 - [8] Andrea Trombettoni and Augusto Smerzi, “Discrete Solitons and Breathers with Dilute Bose-Einstein Condensates,” *Phys. Rev. Lett.* **86**, 2353–2356 (2001).
 - [9] J. C. Eilbeck, P. S. Lomdahl, and A. C. Scott, “The discrete self-trapping equation,” *Physica D: Nonlinear Phenomena* **16**, 318–338 (1985).
 - [10] Eugene P. Gross, “Structure of a quantized vortex in boson systems,” *Il Nuovo Cimento* (1955-1965) **20**, 454–477 (1961).
 - [11] Eugene P. Gross, “Hydrodynamics of a Superfluid Condensate,” *Journal of Mathematical Physics* **4**, 195–207 (1963).
 - [12] L. Pitaevskii and S. Stringari, *Bose-Einstein Condensation* (Oxford University Press, USA, 2003).
 - [13] Lev Davidovich Landau and V. L. Ginzburg, “On the theory of superconductivity,” *Zh. Eksp. Teor. Fiz.* **20**, 1064 (1950).
 - [14] Yoshiki Kuramoto and Dorjsuren Battogtokh, “Coexistence of Coherence and Incoherence in Nonlocally Coupled Phase Oscillators,” *Nonlinear Phenom. Complex Syst* **5**, 380–385 (2002).
 - [15] Yoshiki Kuramoto and Shin-ichiro Shima, “Rotating Spirals without Phase Singularity in Reaction-Diffusion Systems,” *Prog. Theor. Phys. Supplement* **150**, 115–125 (2003).

- [16] Shin-ichiro Shima and Yoshiki Kuramoto, “Rotating spiral waves with phase-randomized core in nonlocally coupled oscillators,” *Phys. Rev. E* **69**, 036213 (2004).
- [17] Pan-Jun Kim, Tae-Wook Ko, Hawoong Jeong, and Hie-Tae Moon, “Pattern formation in a two-dimensional array of oscillators with phase-shifted coupling,” *Phys. Rev. E* **70**, 065201 (2004).
- [18] Erik A. Martens, Carlo R. Laing, and Steven H. Strogatz, “Solvable Model of Spiral Wave Chimeras,” *Phys. Rev. Lett.* **104**, 044101 (2010).
- [19] Adilson E. Motter, “Nonlinear dynamics: Spontaneous synchrony breaking,” *Nat Phys* **6**, 164–165 (2010).
- [20] Chad Gu, Ghislain St-Yves, and Jörn Davidsen, “Spiral Wave Chimeras in Complex Oscillatory and Chaotic Systems,” *Phys. Rev. Lett.* **111**, 134101 (2013).
- [21] Hon Wai Lau and Jörn Davidsen, “Linked and knotted chimera filaments in oscillatory systems,” *Phys. Rev. E* **94**, 010204 (2016).
- [22] Bidesh K. Bera, Soumen Majhi, Dibakar Ghosh, and MatjaÅž Perc, “Chimera states: Effects of different coupling topologies,” *EPL* **118**, 10001 (2017).
- [23] Aaron M. Hagerstrom, Thomas E. Murphy, Rajarshi Roy, Philipp Hövel, Iryna Omelchenko, and Eckehard Schöll, “Experimental observation of chimeras in coupled-map lattices,” *Nature Physics* **8**, 658–661 (2012).
- [24] Mark R. Tinsley, Simbarashe Nkomo, and Kenneth Showalter, “Chimera and phase-cluster states in populations of coupled chemical oscillators,” *Nature Physics* **8**, 662–665 (2012).
- [25] Simbarashe Nkomo, Mark R. Tinsley, and Kenneth Showalter, “Chimera States in Populations of Nonlocally Coupled Chemical Oscillators,” *Phys. Rev. Lett.* **110**, 244102 (2013).
- [26] Erik Andreas Martens, Shashi Thutupalli, Antoine Fourrière, and Oskar Hallatschek, “Chimera states in mechanical oscillator networks,” *PNAS* **110**, 10563–10567 (2013).
- [27] Mahesh Wickramasinghe and István Z. Kiss, “Spatially Organized Dynamical States in Chemical Oscillator Networks: Synchronization, Dynamical Differentiation, and Chimera Patterns,” *PLOS ONE* **8**, e80586 (2013).
- [28] Lennart Schmidt, Konrad Schönleber, Katharina Krischer, and Vladimir García-Morales, “Coexistence of synchrony and incoherence in oscillatory media under nonlinear global coupling,” *Chaos: An Interdisciplinary Journal of Nonlinear Science* **24**, 013102 (2014).
- [29] David P. Rosin, “Transient scaling and resurgence of chimera states in networks of Boolean phase oscillators,” *Phys. Rev. E* **90** (2014).
- [30] Laurent Larger, Bogdan Penkovsky, and Yuri Maistrenko, “Virtual Chimera States for Delayed-Feedback Systems,” *Phys. Rev. Lett.* **111**, 054103 (2013).
- [31] Laurent Larger, Bogdan Penkovsky, and Yuri Maistrenko, “Laser chimeras as a paradigm for multistable patterns in complex systems,” *Nature Communications* **6**, 7752 (2015).
- [32] Tomasz Kapitaniak, Patrycja Kuzma, Jerzy Wojewoda, Krzysztof Czołczynski, and Yuri Maistrenko, “Imperfect chimera states for coupled pendula,” *Scientific Reports* **4**, 6379 (2014).
- [33] Franco Dalfovo, Stefano Giorgini, Lev P. Pitaevskii, and Sandro Stringari, “Theory of Bose-Einstein condensation in trapped gases,” *Rev. Mod. Phys.* **71**, 463–512 (1999).
- [34] Anthony J. Leggett, “Bose-Einstein condensation in the alkali gases: Some fundamental concepts,” *Rev. Mod. Phys.* **73**, 307–356 (2001).
- [35] James R. Anglin and Wolfgang Ketterle, “Bose-Einstein condensation of atomic gases,” *Nature* **416**, 211–218 (2002).
- [36] C. J. Pethick and H. Smith, *Bose-Einstein Condensation in Dilute Gases*, 2nd ed. (Cambridge University Press, 2008).
- [37] Dirk Witthaut and Marc Timme, “Kuramoto dynamics in Hamiltonian systems,” *Phys. Rev. E* **90**, 032917 (2014).
- [38] Helmut Ritsch, Peter Domokos, Ferdinand Brennecke, and Tilman Esslinger, “Cold atoms in cavity-generated dynamical optical potentials,” *Rev. Mod. Phys.* **85**, 553–601 (2013).
- [39] Dan Tanaka and Yoshiki Kuramoto, “Complex Ginzburg-Landau equation with nonlocal coupling,” *Phys. Rev. E* **68**, 026219 (2003).
- [40] J. S. Douglas, H. Habibian, C.-L. Hung, A. V. Gorshkov, H. J. Kimble, and D. E. Chang, “Quantum many-body models with cold atoms coupled to photonic crystals,” *Nat Photon* **9**, 326–331 (2015).
- [41] A. González-Tudela, C.-L. Hung, D. E. Chang, J. I. Cirac, and H. J. Kimble, “Subwavelength vacuum lattices and atom-atom interactions in two-dimensional photonic crystals,” *Nat Photon* **9**, 320–325 (2015).
- [42] Inés de Vega, “Matter-Wave Emission in Optical Lattices: Single Particle and Collective Effects,” *Phys. Rev. Lett.* **101** (2008).
- [43] Carlos Navarrete-Benlloch, Inés de Vega, Diego Porras, and J. Ignacio Cirac, “Simulating quantum-optical phenomena with cold atoms in optical lattices,” *New J. Phys.* **13**, 023024 (2011).
- [44] A. González-Tudela and J. I. Cirac, “Purely Long-Range Coherent Interactions in Two-Dimensional Structured Baths,” *arXiv:1705.10242 [quant-ph]* (2017).
- [45] A. González-Tudela and J. I. Cirac, “Quantum Emitters in Two-dimensional Structured Reservoirs in the Non-Perturbative Regime,” *arXiv:1705.06673 [quant-ph]* (2017).
- [46] D. Jaksch, C. Bruder, J. I. Cirac, C. W. Gardiner, and P. Zoller, “Cold Bosonic Atoms in Optical Lattices,” *Phys. Rev. Lett.* **81**, 3108–3111 (1998).
- [47] Omjyoti Dutta, Mariusz Gajda, Philipp Hauke, Maciej Lewenstein, Dirk-Sören Lühmann, Boris A. Malomed, Tomasz Sowiński, and Jakub Zakrzewski, “Non-standard Hubbard models in optical lattices: a review,” *Rep. Prog. Phys.* **78**, 066001 (2015).
- [48] Renate Landig, Lorenz Hruby, Nishant Dogra, Manuele Landini, Rafael Mottl, Tobias Donner, and Tilman Esslinger, “Quantum phases from competing short- and long-range interactions in an optical lattice,” *Nature* **532**, 476–479 (2016).

- [49] David C. McKay, Carolyn Meldgin, David Chen, and Brian DeMarco, “Slow Thermalization between a Lattice and Free Bose Gas,” *Phys. Rev. Lett.* **111**, 063002 (2013).
- [50] Marlan O. Scully and M. Suhail Zubairy, *Quantum Optics* (Cambridge University Press, 1997).
- [51] Christopher Gerry and Peter Knight, *Introductory quantum optics* (Cambridge university press, 2005).
- [52] D. Jaksch and P. Zoller, “The cold atom Hubbard toolbox,” *Annals of Physics Special Issue*, **315**, 52–79 (2005).
- [53] Oliver Morsch and Markus Oberthaler, “Dynamics of Bose-Einstein condensates in optical lattices,” *Rev. Mod. Phys.* **78**, 179–215 (2006).
- [54] Cheng Chin, Rudolf Grimm, Paul Julienne, and Eite Tiesinga, “Feshbach resonances in ultracold gases,” *Rev. Mod. Phys.* **82**, 1225–1286 (2010).
- [55] Hon Wai Lau, Zachary Dutton, Tian Wang, and Christoph Simon, “Proposal for the Creation and Optical Detection of Spin Cat States in Bose-Einstein Condensates,” *Phys. Rev. Lett.* **113**, 090401 (2014).
- [56] Note that the same pattern can also arise from other initial conditions such as perturbations around the phase singularity (see SM and animation).
- [57] E. Brion, L. H. Pedersen, and K. Mølmer, “Adiabatic elimination in a lambda system,” *J. Phys. A: Math. Theor.* **40**, 1033 (2007).
- [58] E. Nicklas, H. Strobel, T. Zibold, C. Gross, B. A. Malomed, P. G. Kevrekidis, and M. K. Oberthaler, “Rabi Flopping Induces Spatial Demixing Dynamics,” *Phys. Rev. Lett.* **107**, 193001 (2011).
- [59] S. Burger, K. Bongs, S. Dettmer, W. Ertmer, K. Sengstock, A. Sanpera, G. V. Shlyapnikov, and M. Lewenstein, “Dark Solitons in Bose-Einstein Condensates,” *Phys. Rev. Lett.* **83**, 5198–5201 (1999).
- [60] Immanuel Bloch, “Ultracold quantum gases in optical lattices,” *Nat Phys* **1**, 23–30 (2005).
- [61] K. B. Davis, M. O. Mewes, M. R. Andrews, N. J. van Druten, D. S. Durfee, D. M. Kurn, and W. Ketterle, “Bose-Einstein Condensation in a Gas of Sodium Atoms,” *Phys. Rev. Lett.* **75**, 3969–3973 (1995).
- [62] Bryce Gadway, Daniel Pertot, Jeremy Reeves, and Dominik Schneble, “Probing an ultracold-atom crystal with matter waves,” *Nat Phys* **8**, 544–549 (2012).
- [63] Salman Habib, Kosuke Shizume, and Wojciech Hubert Zurek, “Decoherence, Chaos, and the Correspondence Principle,” *Phys. Rev. Lett.* **80**, 4361–4365 (1998).
- [64] N. Henkel, R. Nath, and T. Pohl, “Three-Dimensional Roton Excitations and Supersolid Formation in Rydberg-Excited Bose-Einstein Condensates,” *Phys. Rev. Lett.* **104**, 195302 (2010).
- [65] A. Mari, A. Farace, N. Didier, V. Giovannetti, and R. Fazio, “Measures of Quantum Synchronization in Continuous Variable Systems,” *Phys. Rev. Lett.* **111**, 103605 (2013).
- [66] Tony E. Lee and H. R. Sadeghpour, “Quantum Synchronization of Quantum van der Pol Oscillators with Trapped Ions,” *Phys. Rev. Lett.* **111**, 234101 (2013).
- [67] Stefan Walter, Andreas Nunnenkamp, and Christoph Bruder, “Quantum Synchronization of a Driven Self-Sustained Oscillator,” *Phys. Rev. Lett.* **112**, 094102 (2014).
- [68] V. M. Bastidas, I. Omelchenko, A. Zakharova, E. Schöll, and T. Brandes, “Quantum signatures of chimera states,” *Phys. Rev. E* **92**, 062924 (2015).
- [69] Dirk Witthaut, Sandro Wimberger, Raffaella Burioni, and Marc Timme, “Classical synchronization indicates persistent entanglement in isolated quantum systems,” *Nature Communications* **8**, 14829 (2017).
- [70] David Viennot and Lucile Aubourg, “Quantum chimera states,” *Physics Letters A* **380**, 678–683 (2016).
- [71] Xavier Antoine, Weizhu Bao, and Christophe Besse, “Computational methods for the dynamics of the nonlinear Schrödinger/Gross-Pitaevskii equations,” *Computer Physics Communications* **184**, 2621–2633 (2013).

Acknowledgements

We thank David Hobill, Lindsay Leblanc, Matthew Fisher, Stephen Wein, Farokh Mivehvar, for useful discussions. This research was enabled in part by support provided by WestGrid, Calcul Québec, and Compute Canada. H.W.L. was supported by AITF and NSERC. J.D. and C.S. acknowledge financial support from NSERC.

Author contributions statement

H.W.L. conceived the project, constructed the mathematical models, performed calculations and simulations; J.D. supervised the chimera pattern aspects of the project; C.S. supervised the atomic physics aspects of the project; All authors reviewed the final version of the manuscript.

Additional information

Competing financial interests: The authors declare no competing financial interests.

Supplementary Materials: Chimera patterns in conservative systems and ultracold atoms with mediated nonlocal hopping

ALTERNATIVE HAMILTONIANS OF THE NONLOCAL HOPPING MODEL

The Hamiltonian of the NLHM is given by

$$\mathcal{H} = \frac{U}{2} \sum_i |a_i|^4 - P \sum_{i,j} G_{ji} a_i^* a_j, \quad (\text{S1})$$

with $G_{ij} = G_{ji}$ and $G_{ii} = 0$. This Hamiltonian can be represented in a few different canonical variables (see [S1, S2] for example). Suppose the canonical coordinate and momentum variables are q_i and p_i respectively, then we can define

$$a_i = \frac{1}{\sqrt{2}}(q_i + ip_i), \quad (\text{S2})$$

$$a_i^* = \frac{1}{\sqrt{2}}(q_i - ip_i). \quad (\text{S3})$$

With this transformation, the Hamiltonian becomes

$$\mathcal{H} = \frac{U}{8} \sum_i (q_i^2 + p_i^2)^2 - \frac{1}{2} P \sum_{i,j} G_{i,j} (q_i q_j + p_i p_j), \quad (\text{S4})$$

Similarly, we can define the action and angle to be n_i and θ_i respectively, such that $a_i = \sqrt{n_i} e^{i\theta_i}$, or

$$n_i = \frac{1}{2} (q_i^2 + p_i^2), \quad (\text{S5})$$

$$\theta_i = \tan^{-1} (p_i / q_i). \quad (\text{S6})$$

Now, the Hamiltonian becomes

$$\mathcal{H} = \frac{U}{2} \sum_i n_i^2 - P \sum_{i,j} G_{i,j} \sqrt{n_i n_j} \cos(\theta_j - \theta_i). \quad (\text{S7})$$

Note that n_i may be interpreted as the (mean-field) number of particle at site i . Hence, the conservation of the total number of particles implies the quantities $\sum_i |a_i|^2$, $\sum_i (q_i^2 + p_i^2)$, and $\sum_i n_i$ are constant. Moreover, the Hamiltonian is invariant under the transformation $a_i \rightarrow a_i e^{i\theta_0}$ with arbitrary global phase.

In the continuum limit, such as the adiabatic elimination of the simplest two-component model in the the main text, the corresponding Hamiltonian can be obtained by replacing $a_i \rightarrow \psi(\mathbf{r})$, $\sum_i \rightarrow \int d\mathbf{r}$, $\sum_{i,j} \rightarrow \int \int d\mathbf{r} d\mathbf{r}'$ and $G_{i,j} \rightarrow G(\mathbf{r}, \mathbf{r}')$. Explicitly, the Hamiltonians are:

$$\mathcal{H} = \frac{U}{2} \int d\mathbf{r} |\psi(\mathbf{r})|^4 - P \int \int d\mathbf{r} d\mathbf{r}' G(\mathbf{r}, \mathbf{r}') \psi^*(\mathbf{r}) \psi(\mathbf{r}'), \quad (\text{S8})$$

$$\mathcal{H} = \frac{U}{8} \int d\mathbf{r} (q(\mathbf{r})^2 + p(\mathbf{r})^2)^2 - \frac{1}{2} P \int \int d\mathbf{r} d\mathbf{r}' G(\mathbf{r}, \mathbf{r}') (q(\mathbf{r})q(\mathbf{r}') + p(\mathbf{r})p(\mathbf{r}')), \quad (\text{S9})$$

$$\mathcal{H} = \frac{U}{2} \int d\mathbf{r} (n(\mathbf{r}))^2 - P \int \int d\mathbf{r} d\mathbf{r}' G(\mathbf{r}, \mathbf{r}') \sqrt{n(\mathbf{r})n(\mathbf{r}')} \cos(\theta(\mathbf{r}') - \theta(\mathbf{r})). \quad (\text{S10})$$

HOPPING IN ULTRACOLD ATOMS WITH A PERIODIC LATTICE

We start from the equations in the main paper:

$$i\hbar \dot{\psi}_1(\mathbf{r}, t) = (-\hbar\kappa \nabla^2 + V_1 + g_{11}|\psi_1|^2) \psi_1 + \hbar\Omega \psi_2, \quad (\text{S11})$$

$$i\hbar \dot{\psi}_2(\mathbf{r}, t) = (-\hbar\kappa \nabla^2 + \hbar\Delta_2) \psi_2 + \hbar\Omega \psi_1. \quad (\text{S12})$$

In general, adiabatic elimination works best when the first component evolves the slowest [S3]. However, no such choice exist for an arbitrary wavefunction of Eq. (S11), but it exists when the dynamics are confined to the lowest energy band since the excitations have fast dynamics. We derive the effective model with these two assumptions.

Note that there is no basis that is simultaneously good for both equations; although, the good basis for the localized and mediating equation are the Wannier basis and Fourier basis respectively. For the system here, it is easier to understand in the Wannier basis $\{w_{mn}(\mathbf{r})\}$ [S4, S5] for a periodic lattice, where n is the energy band index and m is the lattice site index. In this new basis, the wavefunctions can be represented by $\psi_1(\mathbf{r}, t) = \sum_{mn} a_{mn}(t)w_{mn}(\mathbf{r})$ and $\psi_2(\mathbf{r}, t) = \sum_{mn} b_{mn}(t)w_{mn}(\mathbf{r})$ respectively. Substituting the transformation back into Eq. (S11) and (S12), we have

$$i\hbar\dot{a}_{mn}(t) = \epsilon_{mn}a_{mn} + U|a_{mn}|^2a_{mn} + \hbar\Omega b_{mn}, \quad \text{for } n = 1, \quad (\text{S13})$$

$$i\hbar\dot{b}_{mn}(t) = \hbar\sum_{kl} c_{mnkl}b_{kl} + \hbar\Delta_2 b_{mn} + \hbar\Omega a_{mn}, \quad (\text{S14})$$

where

$$\epsilon_{mn} = \int_V d\mathbf{r} (\hbar\kappa|\nabla w_{mn}|^2 + V_1|w_{mn}|^2), \quad (\text{S15})$$

$$U = g_{11} \int_V d\mathbf{r} |w_{mn}|^4, \quad (\text{S16})$$

$$c_{mnkl} = \kappa \int_V d\mathbf{r} \nabla w_{mn}^*(\mathbf{r}) \nabla w_{kl}(\mathbf{r}), \quad (\text{S17})$$

Note that we assume $a_{mn} = 0$ for all $n > 1$. We also assume that the trap potential V_1 is sufficiently deep so that there is no direct hopping. In this setting, the eigenenergy $\epsilon_{m1} = \epsilon_0$ is a constant. Hence, we can shift the energy $\Delta_2 \rightarrow \Delta := \Delta_2 - \epsilon_0/\hbar$ using the transformation $a_{mn} \rightarrow a_{mn}e^{-i\epsilon_0 t}$. If the energy gap is large $\epsilon_{m2} - \epsilon_{m1} \gg \hbar\Delta$, then we can ignore the resonance with the higher band index $n > 1$. Furthermore, with initially empty excited states, i.e. $a_{mn}(t=0) = 0$ for $n > 1$, no excited states will be populated because there are no resonance with those states. Written explicitly:

$$i\hbar\dot{a}_{m1}(t) = U|a_{m1}|^2a_{m1} + \hbar\Omega b_{m1}, \quad (\text{S18})$$

$$i\hbar\dot{b}_{m1}(t) = \hbar\sum_{kl} c_{m1kl}b_{kl} + \hbar\Delta b_{m1} + \hbar\Omega a_{m1}, \quad (\text{S19})$$

$$i\hbar\dot{b}_{mn}(t) = \hbar\sum_{kl} c_{mnkl}b_{kl}, \quad \text{for } n > 1. \quad (\text{S20})$$

In this form, all the important dynamics are captured, and the localized component can be slow relative to the mediating component.

HOPPING KERNELS WITH A LATTICE

Suppose the mediating channel has a much faster time scale, so the adiabatic elimination is the same as setting $\dot{b}_{mn} = 0$. Therefore, the hopping kernel can be found by solving b_{m1} in the following self-consistently equation by having $a_{m1} = 1$ at the center:

$$0 = \sum_{kl} c_{m1kl}b_{kl} + \Omega a_{m1} + \Delta b_{m1}, \quad (\text{S21})$$

$$0 = \sum_{kl} c_{mnkl}b_{kl} \quad \text{for } n > 1,$$

This is the discrete analogue of finding the continuous hopping kernel $G_D(\mathbf{r})$ as described in the main text by setting $\psi_1(\mathbf{r}) = \delta(\mathbf{r})$, except the interconversion only happens in certain regions. The effective conversion regions have a length scale 2ℓ of the localized wavefunction, in each lattice unit with length d . Therefore, it is expected that the solution G_{ij} takes a similar form as the continuous system with an effective scaling $\Delta \rightarrow \Delta_{eff} = (2\ell/d)^D \Delta$. Hence, the solution is $b_{i1} = \frac{\Omega}{\Delta} G_{ij} * a_{j1}$. Substituting back into the first component, the hopping strength becomes

$$P = \hbar \frac{\Omega^2}{\Delta}, \quad (\text{S22})$$

the same as the continuous system, and G_{ij} takes the same form as in the Table 1 in the main text. The characteristic hopping radius is

$$R = C_D \left(\frac{d}{2\ell} \right)^{\frac{D}{2}} \sqrt{\frac{\kappa}{\Delta}}, \quad (\text{S23})$$

where D is the dimension and C_D is a constant.

The results above can be verified numerically. This requires a method to find the hopping kernel in a periodic lattice self-consistently. Here, we solve the corresponding time dependent equation of Eq. (S21) and the solution is given by the equilibrium state. Hence, Eq. (S21) with the time splitting method becomes

$$\dot{b}_{m1}(t) = -\Omega a_{m1} - \Delta b_{m1}, \quad (\text{S24})$$

$$\dot{\tilde{\psi}}_2(\mathbf{q}, t) = -\frac{\hbar q^2}{2m} \tilde{\psi}_2, \quad (\text{S25})$$

for the conversion step and propagation step respectively, so the basis is changed between each step. $\tilde{\psi}_2(\mathbf{q}, t)$ is the wavefunction in Fourier space. The hopping kernel G_{ij} is the same as the equilibrium solution b_{i1}^* with $G_{mj} \sim b_{m1}^*$, if the system is set to $a_{m1} = \delta_{j1}$, where j is the source lattice site (chosen to be the center of the lattice). For simplicity, Gaussian approximation is used to approximate the lowest band Wannier function as

$$w_{m1}(\mathbf{r}) = \phi(\mathbf{r} - \mathbf{r}_m) \sim e^{-\frac{\pi|\mathbf{r}-\mathbf{r}_m|^2}{2\ell^2}}, \quad (\text{S26})$$

which is a good approximation when $\ell \ll d$, such as deep sinusoidal trap, where \mathbf{r}_m is the center of the Gaussian. The transformation between real space and Wannier basis are given by

$$b_{m1} = \langle w_{m1}(\mathbf{r}) | \psi_2(\mathbf{r}) \rangle = \int_V d^3\mathbf{r} \phi(\mathbf{r}) \psi_2(\mathbf{r}), \quad (\text{S27})$$

where V is the lattice volume around the lattice minimum $[-d/2, d/2]^D$ with finite cutoff of lattice spacing d .

The numerical results fit perfectly for the kernel $G_D(r)$ in both 1D and 2D as shown in Fig. S1. Moreover, the predicted hopping radius R fit perfectly with Eq. S23 when the Gaussian $\ell \ll d$ is sufficiently narrow such that the approximation is good. Both of these fitting give the constant $C_D \approx 1$.

CHIMERA PATTERNS IN THE NLHM

The dynamics of a system with the spiral initial condition used in the main text is given in Fig. S2 (and an animation). As shown in the figure, the incoherent core is spontaneously formed near the spatial phase singularity. This dynamic pattern is essentially invariant under the scale of system with fixed R/L as shown in Fig. S3, which has both system size L and hopping radius R four times larger. The core has locally incoherent phase, while the dynamics outside the core are locally coherent. These chimera core patterns can also arise from alternative initial conditions, such as a vortex with a randomized core as shown in Fig. S4.

The dynamics are very different when the hopping range becomes small $R \sim d$. With only nearest-neighbors hopping, the system becomes the discrete Gross-Pitaevskii equation. The difference is very clear when the system is started from the same random core with nearest-neighbor hopping as shown in Fig. S5. The random phase near the core is a localized perturbation that propagates outward like a wave and interferes with itself. In this case, no localized chimera core can be observed.

Noise

The behaviour of the core is very different from the background. In particular, the dynamics of the core are very sensitive to small fluctuations or noises. For example, we can evolve the system backward in time and expect it to go back to the initial spiral, as shown in S6a, if the system starts from the state in Fig. S2f. The sensitivity of the core region can be tested by adding a small single-shot noise

$$a_i \rightarrow a_i + \chi_{\text{noise}} \xi_i, \quad (\text{S28})$$

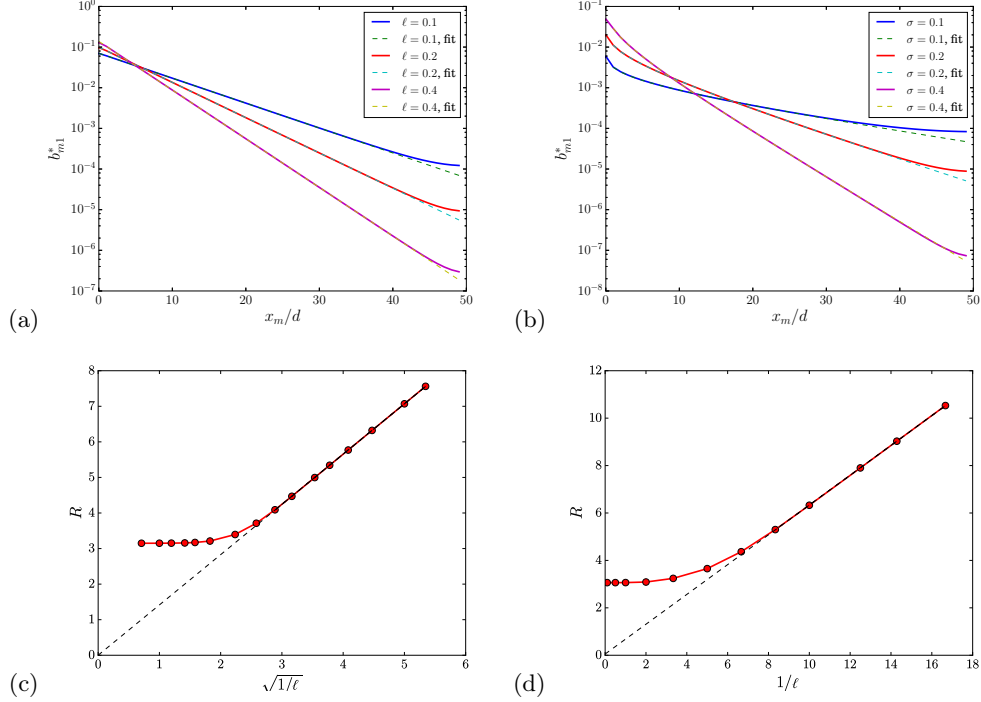


Figure S1: Discrete hopping kernel G_{ij} . (a) Comparing the numerical kernel b_{m1}^* with exponential fitting in 1D. $\kappa = 100$, $\Omega = 10$, and $\Delta = 10$. (b) Comparing b_{m1}^* with K_0 fitting in 2D. (c) The scaling of the hopping radius $R \sim \ell^{-1/2}$ in 1D versus a length scale ℓ . (d) The scaling of the hopping radius $R \sim \ell^{-1}$ in 2D versus ℓ .

where the noise is Gaussian with $\langle \xi_i \rangle = 0$, $\langle \text{Re}(\xi_i) \text{Re}(\xi_{i'}) \rangle = \delta_{i,i'}$, and $\langle \text{Im}(\xi_i) \text{Im}(\xi_{i'}) \rangle = \delta_{i,i'}$, with amplitude χ_{noise} . This noise can be added to the state in Fig. S2f as a perturbation before the backward propagation. As shown in Fig. S6b and S6c, the system cannot go back to the spiral even with a noise as low as $\chi_{\text{noise}} = 10^{-11}$, as compared to the order $\mathcal{O}(1)$ of the amplitude and phase. This suggests that the core region is very sensitive to the initial condition. This is in stark contrast to with the behaviour of the coherent background, which can go back to the same local states as in the noiseless case.

Loss

The nonlinear particle loss can be modelled by the replacing $U \rightarrow U - iU_{\text{loss}}$. Therefore, the dynamic equation with loss is

$$i\hbar \dot{a}_i = (U - iU_{\text{loss}})|a_i|^2 a_i - P \sum_j G_{ij} a_j. \quad (\text{S29})$$

The particle loss can be calculated by the time-derivative of the total number of particles:

$$\frac{dN}{dt} = \frac{d}{dt} \sum_i |a_i|^2 = \sum_i (\dot{a}_i^* a_i + a_i^* \dot{a}_i) = \sum_i - \left(2 \frac{U_{\text{loss}}}{\hbar} \right) |a_i|^4, \quad (\text{S30})$$

where the dynamic equations for \dot{a}_i and \dot{a}_i^* are substituted above. Suppose all lattice sites have the same number of particles $|a_i|^2 = n$, then the equation becomes

$$\frac{dn}{dt} = - \left(2 \frac{U_{\text{loss}}}{\hbar} \right) n^2. \quad (\text{S31})$$

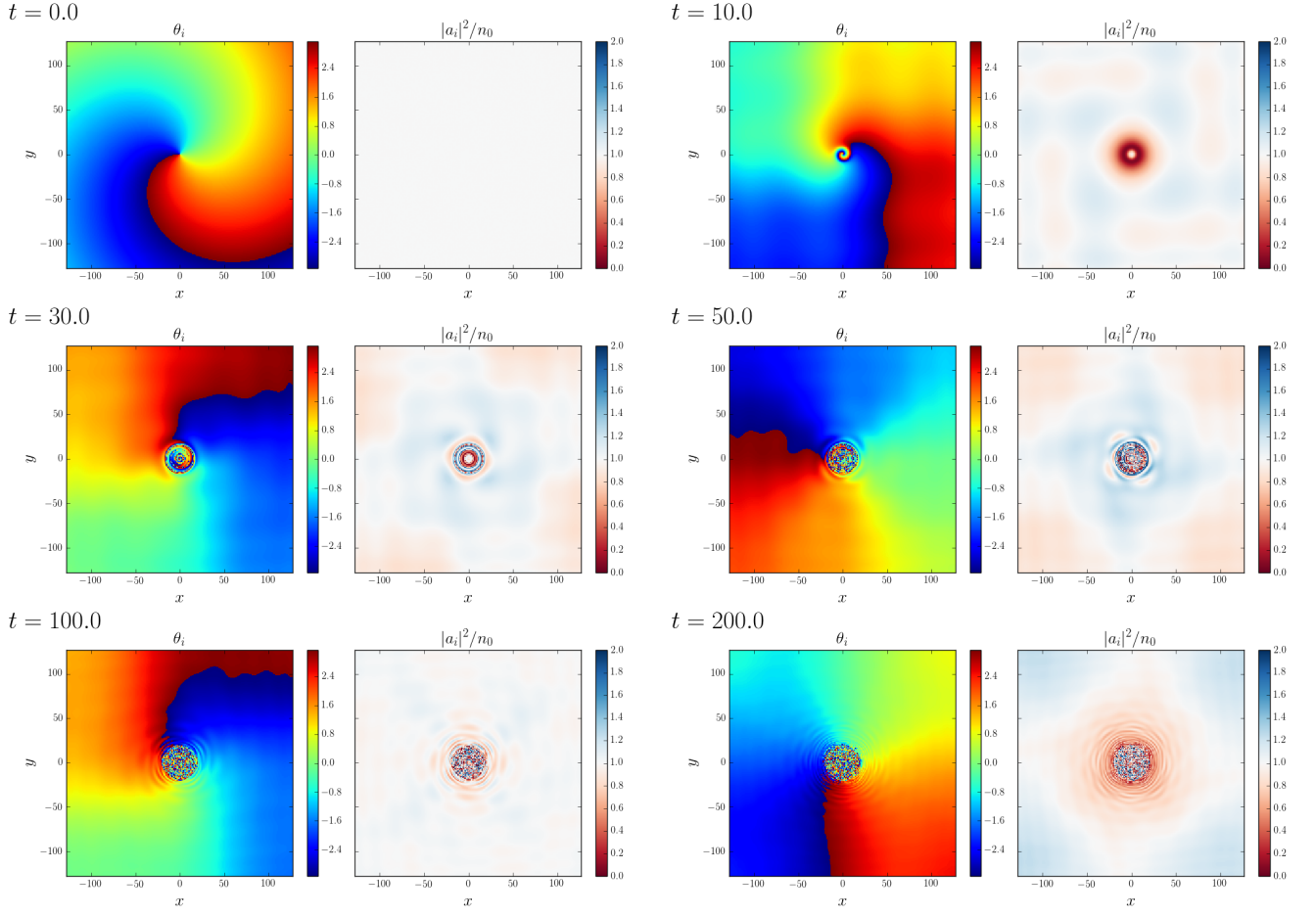


Figure S2: Time evolution of the initial spiral with $k_s = 0.01$. We used nonlocal hopping $P/(Un_0) = 0.5$ and $R = 16$ in a system with a lattice size of $L = 256$.

Let $\chi = 2U_{loss}/\hbar$ and then by solving the equation, we have

$$n(t) = \frac{1}{n_0^{-1} + \chi t}, \quad (\text{S32})$$

where n_0 is the initial number of particles per site. Suppose n_0 is very large, then the time for half of the particle to become lost is $\chi t = 2$ or $U_{loss}t/\hbar = 1$. As shown in Fig. S7, the phase of the chimera patterns changes only slightly compared to the lossless case on timescales where many more than half of the particles remain in the system.

-
- [S1] D. Witthaut and M. Timme, Phys. Rev. E **90**, 032917 (2014).
 - [S2] Q. Thommen, J. C. Garreau, and V. Zehnlé, Phys. Rev. Lett. **91**, 210405 (2003).
 - [S3] E. Brion, L. H. Pedersen, and K. Mølmer, J. Phys. A: Math. Theor. **40**, 1033 (2007).
 - [S4] D. Jaksch, C. Bruder, J. I. Cirac, C. W. Gardiner, and P. Zoller, Phys. Rev. Lett. **81**, 3108 (1998).
 - [S5] O. Morsch and M. Oberthaler, Rev. Mod. Phys. **78**, 179 (2006).

$t = 100.0$

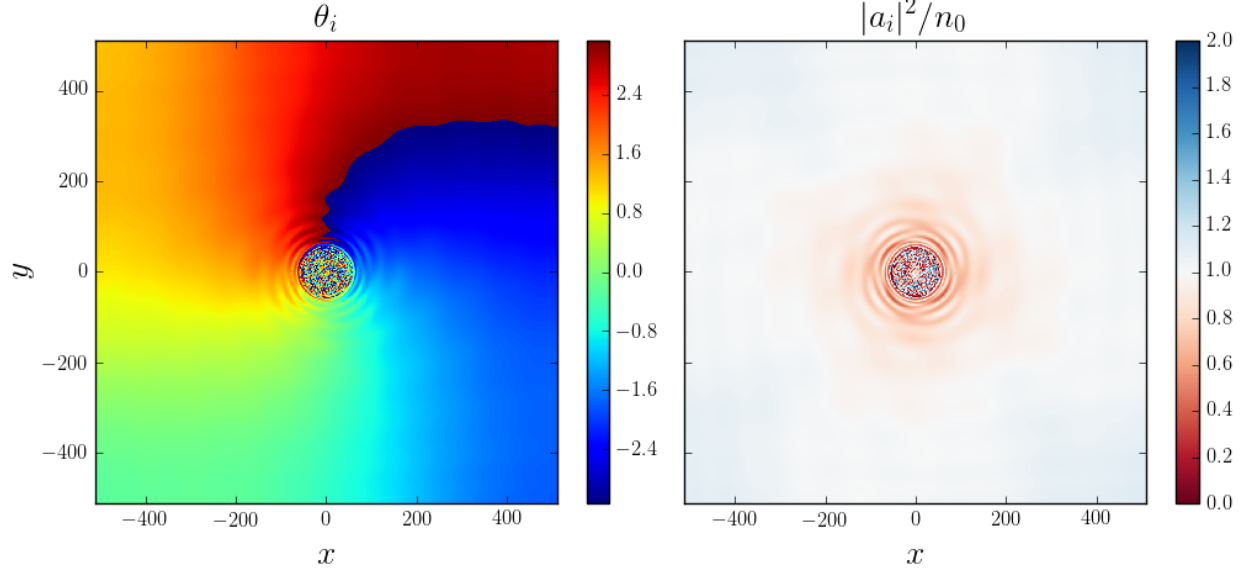
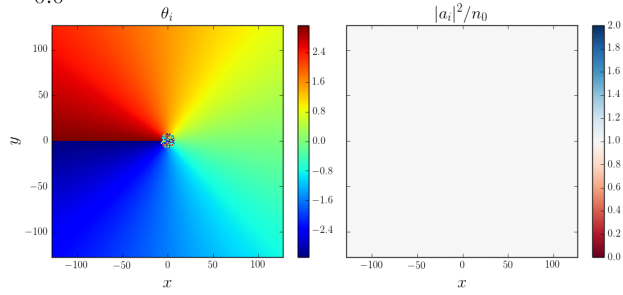


Figure S3: Similar to Fig. S2 but in a larger system with initial spiral $k_s = 0.0025$. We use nonlocal hopping $P/(Un_0) = 0.5$ and $R = 64$ in a system with a lattice size of $L = 1024$. This can be compared with Fig. S2e.

$t = 0.0$



$t = 200.0$

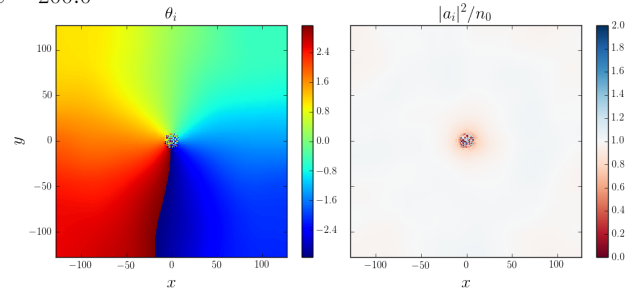


Figure S4: Time evolution of an initial vortex with a random core. $P/(Un_0) = 0.5$, $R = 16$, and $L = 256$.

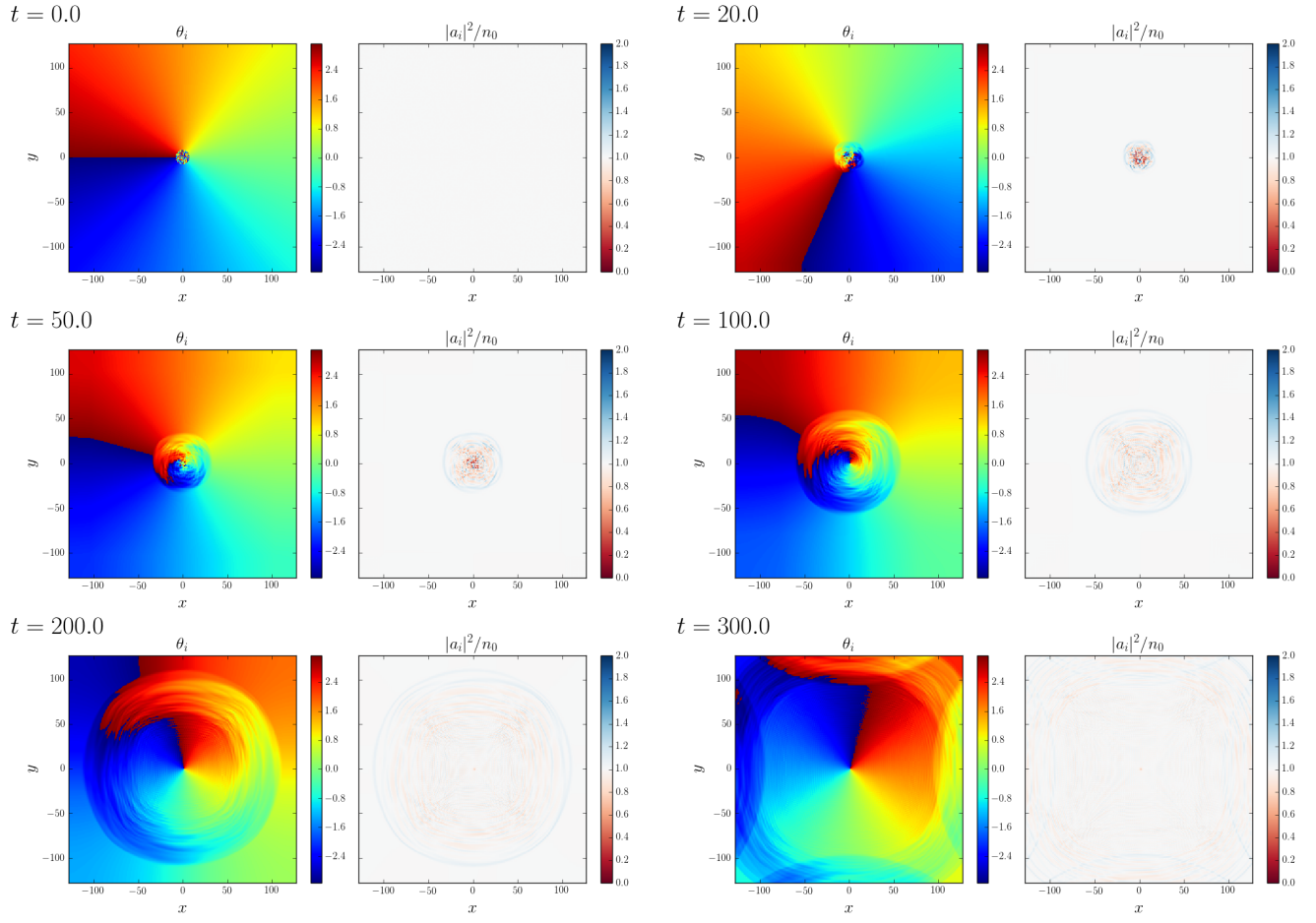


Figure S5: Time evolution of an initial random core with only nearest-neighbor hopping. $P/(Un_0) = 0.5$ and $L = 256$.

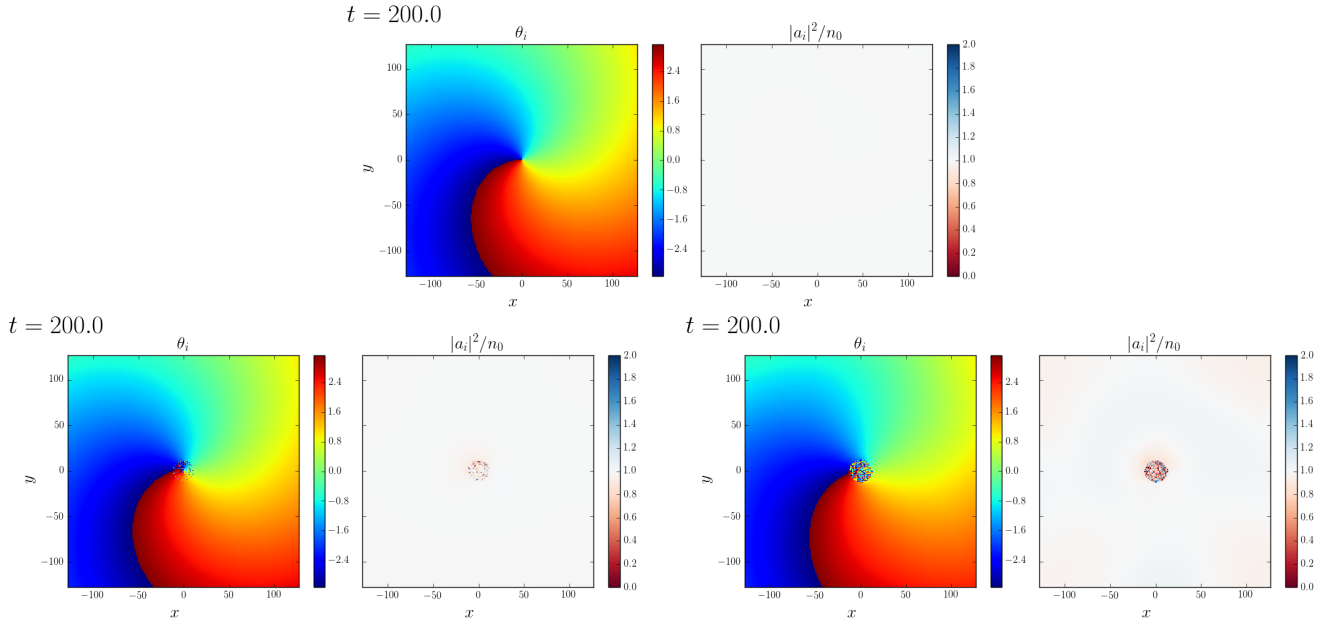


Figure S6: Backward time propagation from the state in Fig. S2f. (a) No noise, (b) $\chi_{noise} = 10^{-11}$, (c) $\chi_{noise} = 10^{-10}$, where the single-shot noises are added before the backward propagation. The noise added is very tiny $\chi_{noise}/|a_i| \sim \chi_{noise}$ since $|a_i| \sim 1$ is used.

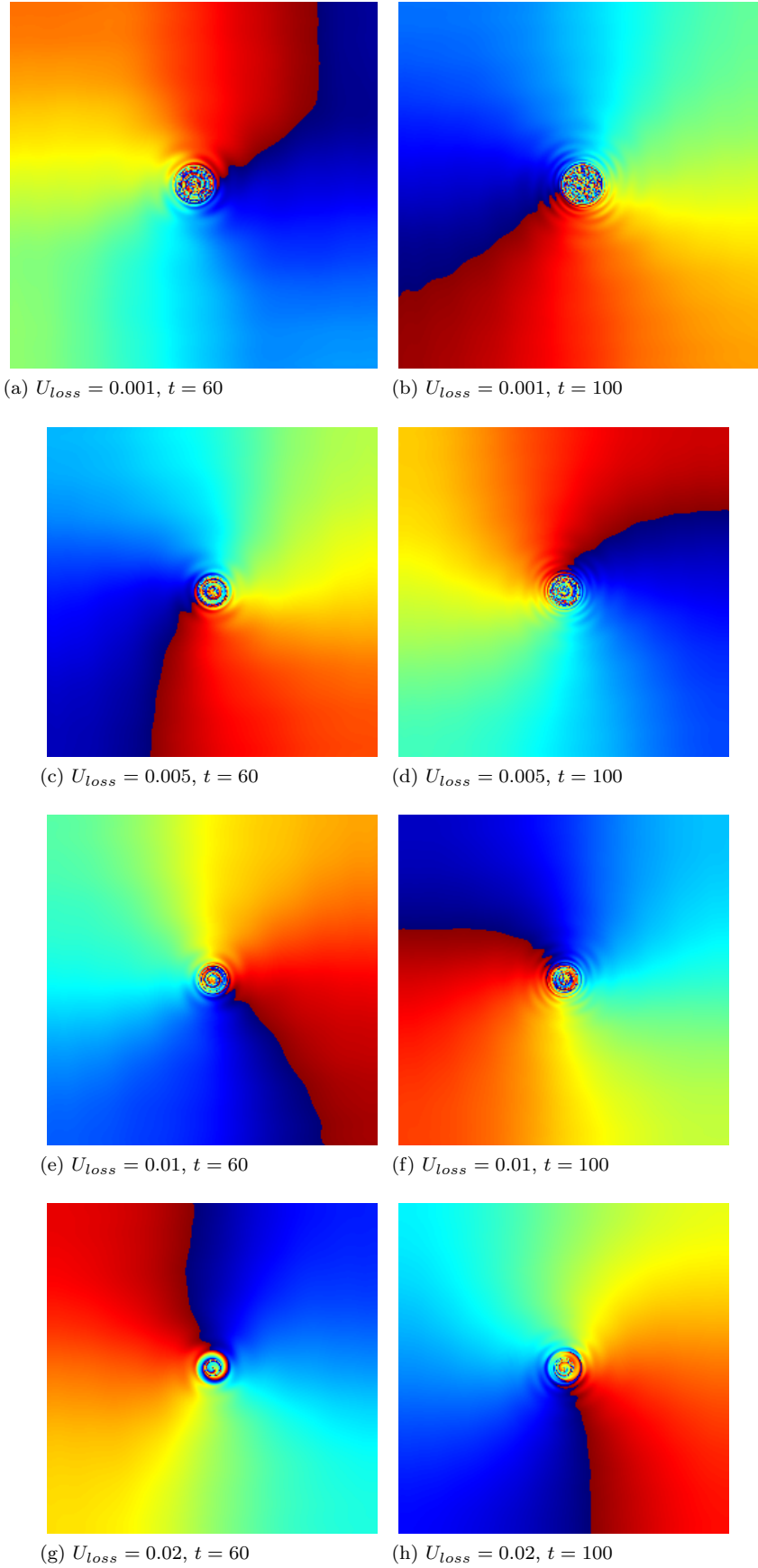


Figure S7: Similar to Fig. S2 with loss $U_{loss} = 0.001, 0.005, 0.01, 0.02$. (left) $t = 60$, (right) $t = 100$. Parameters: $U = 1$, $n_0 = 1$, $P = 0.5$, $R = 16$, and $L = 256$.